A simplified mathematical study of preparation of a particle oxide by a thermo-chemical technique with counter-flow configuration for use in biomedical applications

Amir Tabaei[1], Sadegh Sadeghi[1], Saman Hosseinzadeh[1], Mehdi Bidabadi[1], Qingang Xiong[2, *], Nader Karimi[3]

[1]School of Engineering, Mechanical Engineering Department, Iran University of Science and Technology, Narmak, Tehran, Iran

[2]IT Innovation Center, General Motors, Warren, MI 48092, USA

[3]School of Engineering, University of Glasgow, Glasgow, UK

[*]Corresponding author. Email: qgxiong@126.com (Q. Xiong)

Abstract This study mathematically presents a counter-flow non-premixed thermo-chemical technique for preparing a particle oxide used for cancer diagnosis and treatment. For this purpose, preheating, reaction, melting, and oxidation processes were simulated considering an asymptotic concept. Mass and energy conservation equations in dimensional and non-dimensional forms were solved using Matlab®. To preserve the continuity in the system and calculate the locations of melting and flame fronts, promising jump conditions were derived. In this research, variations of flame temperature, flame front location and mass fractions of the particle, particle oxide and oxidizer, with position, Lewis number and initial temperature of the particles were investigated. The simulation results compared with those obtained from an earlier experimental study under the

same conditions. Regarding the comparison, an appropriate compatibility was observed between the results. Based on the simulation results, flame temperature was found to be about 1310 K. Positions of flame and melting fronts were found to be -1.8 mm and -1.78 mm, respectively.

Keywords: Biomedical applications; Cancer diagnosis and treatment; Particle oxide; Non-premixed mode; Numerical simulation; Counter-flow design.

Nomenclature

a	Strain rate ($\frac{1}{\mathrm{a}}$)
C	Mixture specific heat capacity $\left(\frac{\mathrm{kJ}}{\mathrm{kg.K}}\right)$
C_a	Heat capacity of the gas $\left(\frac{\mathrm{kJ}}{\mathrm{kg.K}}\right)$
C_p	Heat capacity of particle $\left(\frac{\mathrm{kJ}}{\mathrm{kg.K}}\right)$
D_C	Damkohler number
D_F	Diffusion coefficient of particle ($\frac{\mathrm{m}^2}{\mathrm{s}}$)
D_m	Diffusion coefficient of particle oxide in liquid phase ($\frac{\mathrm{m}^2}{\mathrm{s}}$)
D_O	Diffusion coefficient of oxidizer ($\frac{\mathrm{m}^2}{\mathrm{s}}$)
D_T	Thermal diffusion coefficient ($\frac{\mathrm{m}^2}{\mathrm{s}}$)
E	Overall activation energy (kJ)

$erf(x)$	Error function
H	Heaviside function
Le	Lewis number
m	Mixture molecular mass ($\frac{\mathrm{kg}}{\mathrm{mol}}$)
m_F	Fuel molecular mass ($\frac{\mathrm{kg}}{\mathrm{mol}}$)
m_O	Oxidizer molecular mass ($\frac{\mathrm{kg}}{\mathrm{mol}}$)
n_p	Local number density of particles (number of particles per unit volume)
Q	Heat of reaction $\left(\frac{\mathrm{kJ}}{\mathrm{kg}}\right)$
Q_{melt}	Latent heat of melting $\left(\frac{\mathrm{kJ}}{\mathrm{kg}}\right)$
q_{melt}	Ratio of latent heat of melting to the heat released from reaction
R	The universal gas constant $\left(\frac{\mathrm{m^3 Pa}}{\mathrm{mol.K}}\right)$
r_p	Particle radius (μm)
T	Temperature (K)
T_a	Activation temperature (K)
T_{ad}	Adiabatic temperature (K)
T_f	Flame temperature (K)
T_{ig}	Ignition temperature of particles (K)

T_{melt}	Melting temperature of particle oxide (K)
T_{∞}	Ambient temperature (K)
$\mathcal{W}_F$	Molecular weight of particle $\left(\frac{\text{kg}}{\text{kmol}}\right)$
x	Dimensional length (m)
x_f	Dimensional flame sheet position (m)
X_f	Non-dimensional flame sheet position
x_{melt}	Onset position of melting in dimensional form (m)
X_{melt}	Onset position of melting in non-dimensional form
Y_m	Mass fraction of particle oxide in liquid phase
Y_O	Mass fraction of the oxidizer
Y_S	Mass fraction of the particle
$Y_{S-\infty}$	Mass fraction of the particle at the distance $-\infty$
y_m	Dimensionless form of the mass fraction of particle oxide in liquid phase
y_O	Dimensionless form of the mass fraction of oxidizer
y_S	Dimensionless form of the mass fraction of particle

Greek Symbols

ω_{melt}	Melting rate of particle oxide $\left(\frac{\text{kg}}{\text{m.s}^2}\right)$

$\widetilde{\omega}_{melt}$	Dimensionless form of melting
ω_S	Reaction rate $\left(\frac{\text{kg}}{\text{m.s}^2}\right)$
$\widetilde{\omega}_S$	Dimensionless form of the reaction rate
τ_{melt}	Constant characteristic time of melting
λ	Thermal conductivity $\left(\frac{\text{kJ}}{\text{m.s.K}}\right)$
ρ	Density of the mixture $\left(\frac{\text{kg}}{\text{m}^3}\right)$
ρ_a	Density of gas $\left(\frac{\text{kg}}{\text{m}^3}\right)$
ρ_p	Density of particle $\left(\frac{\text{kg}}{\text{m}^3}\right)$
θ	Dimensionless form of the temperature
θ_f	Dimensionless form of flame temperature
θ_{melt}	Dimensionless form of melting temperature
v_O	Oxidizer stoichiometric coefficient
v_p	Product stoichiometric coefficient
v_S	Fuel stoichiometric coefficient

Subscripts

a	Gas
f	Flame

melt	Melting
P	Product
S	Particle
V	Velocity
∞	Ambient condition

1. Introduction

Some particles with magnetism have found wide applications in various areas, especially bioengineering and medicine, e.g., cell separation, detection and treatment of diseases [1-5]. The particles oxide exhibits many unique characteristics, such as small settling velocity, high stability, biocompatibility, nontoxicity and high surface efficiency to attach ligands [2,6,7]. Efficient preparation of particle oxide is the basement of its subsequent practical applications. In general, the particle oxide can be synthesized by different ways, such as combustion, chemical co-precipitation, emulsion, pyrolysis, sol-gel, fluid injection, vaporization, and hydrothermal [8,9]. Among these methods, preparation using flames has been dominant, where the particles react with air or pure oxygen during the burning/flaming process [10-13]. Particle oxide production through flame can overall be divided into premixed and non-premixed modes, where whether the particles and oxygen agents are premixed is the key difference [14]. These two types of flame-based operation have both been widely employed in particle oxide preparation in laboratory and industry for biomedical applications. Different numerical solutions have been proposed to investigate complex heat transfer and fluid dynamics engineering problems [15-19].

Up to now, a sheer volume of experimental studies have been devoted to analyze and test different techniques for production of different particle oxides for biomedical applications. Daoush [20] employed co-precipitation method to form particle oxide for biomedical use in presence of ethylenediaminetetraacetic acid and sodium hydroxide as a precipitating agent considering size and shape of particle. Mata-Pérez et al. [21] invented a simple three-step technique for producing stable and uniform particle oxide at low temperatures by means of x-ray diffraction (XRD), Fourier transform infrared spectroscopy (FT-IR), transmission electron microscopy (TEM), and vibrating sample magnetometry (VSM). Andrade et al. [22] used a direct reduction-precipitation method to form size-controlled particle oxide and examine the impacts of aging time and temperature on the size and monodispersion features of the synthesized oxide. Setyawan and Widiyastuti [23] applied an electrochemical technique by passing an electric current through an anode and a cathode in an electrolyte solution to form a particle oxide. Dresco et al. [24] proposed a two-step microemulsion process and a seed precipitation polymerization for creating particle oxide with different diameters. Koushika et al. [25] used a thermal plasma approach to produce particle oxide powder considering phase and chemical composition of particles. Rashid et al. [26] used an in-situ precipitation strategy to create particle oxide aplying X-ray diffraction, energy-dispersive X-ray spectroscopy and Raman spectroscopy. Silva et al. [27] introduced a precipitation/photoreduction coupled process to form particle oxide for alleviating environmental concerns occurring in coal mines. Lei and Girshick [28] employed a DC thermal plasma approach to synthesize particle oxide by means of aerosol sampling probe connected with a scanning mobility particle sizer for determining the particle size distribution. Owens et al. [29] proposed several sol-gel approaches for synthesizing particle oxide for use in biomedical industry. From these numerical and experimental activities

proposed for production of particle oxides for biomedical applications, it can be clearly seen that investigation of thermo-chemical techniques have hardly been touched.

To this end, a fundamental but in-depth understanding of the underlined mechanisms for preparation of particle oxide under non-premixed mode is of vital importance. However, from the foregoing comprehensive literature review and to the best of our knowledge, few studies have been reported on synthesizing particle oxide under non-premixed conditions. Though there are several reports on numerical simulations of non-premixed combustion of other materials such as biomass [30] and coal [31], analytical study on particles and their oxides used in biomedical industry seems unavailable.

The main objective of this article is to use a simplified numerical model to investigate thermo-chemical technique for producing of a particle oxide for use in biomedical industry. The major stages considered for chemical processing the particles include preheating, reaction, melting, and oxidation processes. Mass and energy conservation equations of each stage in dimensional and non-dimensional forms were formulated and solved through Matlab®. To reveal the locations of flame and melting fronts, appropriate boundary and jump conditions were proposed. The numerical simulation was first validated by experimental data. Then, characteristics in this course, including temperature and front location of flame, mass fractions of the particle, particle oxide and oxidizer are presented. Finally, the effects of Lewis number and initial temperature of the particles are discussed.

2. System description

In this study, it is assumed that oxidizer and particles suspended in an inert gas are injected into the chamber from two distinct nozzles located at $+\infty$ and $-\infty$, respectively. Mixture of the

fuel and oxidizer is ignited by an electric spark. Several processes including preheating, oxidation, and melting are considered in this study. The model for combustion of single particle is illustrated in Fig. 1. Regarding the figure, after preheating process, when a single particle meets the oxidizer, oxidizer molecules are slowly adsorbed on the surface of the particle. Oxidizer molecules are physically dissociated and chemically adsorbed on the oxide surface. Reaction occurs at the particle-oxide interface in a very thin zone. It is notable that the reaction zone propagates towards the core of the particle and molten particle oxide is produced outside the reaction zone, as can be seen in Fig. 1.

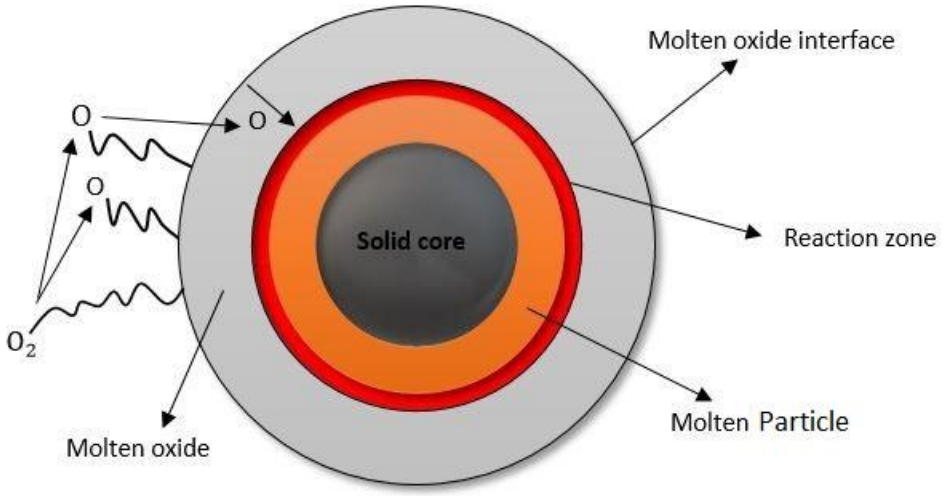

Fig. 1 Oxidation process of a single particle.

Structure of the counter-flow non-premixed flame formed by micron-sized particles is shown in Fig. 2. As can be seen in this figure, the combustion system consists of several zones including preheating, reaction, melting, and oxidizer zones. In the preheating zone, in absence of oxidizer, particles are heated and their temperature increases gradually. As the particles collide with the oxidizer stream and gain required activation energy, the particles asymptotically combust

and reaction occurs, leading to the formation of particle oxide. Afterwards, all of the particle oxide are asymptotically melted. Eventually, molten particle oxide are converted into solid phase by rejecting heat to the oxidizer stream, and exit the system. Momentum of the particles (accompanied by an inert gas) and oxidizer stream are presumed to be constant. Therefore, a stagnation line, as shown in Fig. 2, is located in the middle of the distance between particle and oxidizer nozzles. In this study, positions of flame and melting fronts are measured relative to the location of stagnation line.

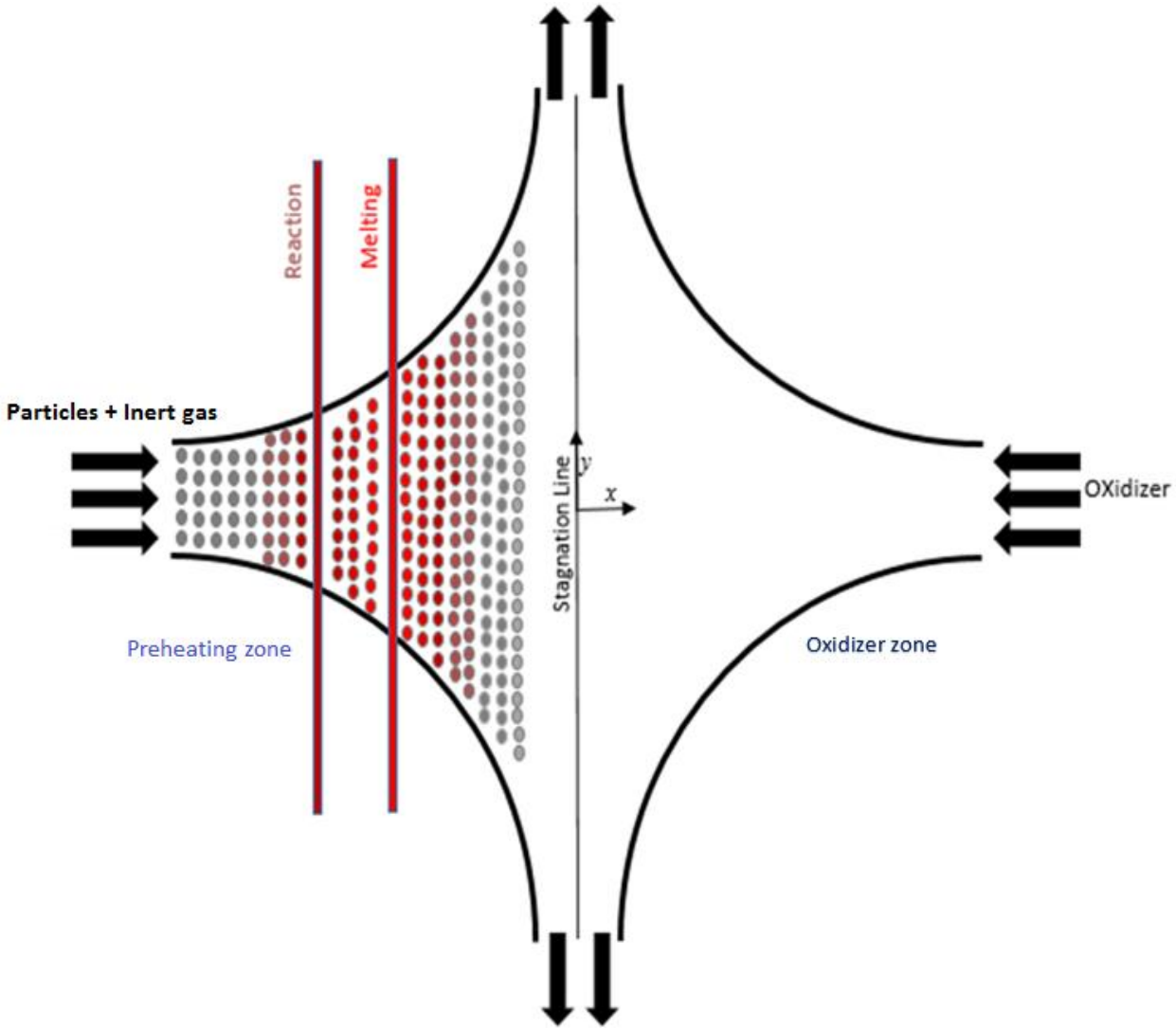

Fig. 2 Structure of the counter-flow non-premixed combustion of the particles.

3. Theoretical modeling

3.1. Mathematical modeling of the reaction and melting processes

Reaction process occurs within a very thin zone as the value of Zeldovich number is considered to be very large. The one-stage Arrhenius model is used to describe the reaction process as [32]

$$v_F[F] + v_O[O] \rightarrow v_{product}[P] \quad (1)$$

where $[F]$, $[O]$, and $[P]$ represent fuel, oxidizer, and products, respectively. Also, v_F, v_O and v_P are stoichiometric coefficients of fuel, oxidizer and products, respectively. Rate of reaction is formulated as [32]

$$\omega_S = B\rho^2 v_F\, v_O \overline{Y_S}\,\overline{Y_O} exp\left(-\frac{E_a}{RT_f}\right) \quad (2)$$

where Y_S, Y_O, ρ, B, E_a, R, and T_f are mass fraction of particles, mass fraction of oxidizer, density of mixture, frequency factor, activation energy, universal gases constant (R=8.314 $\frac{J}{mol\ K}$), and flame temperature, respectively. The following equations are used to calculate $\overline{Y_S}$ and $\overline{Y_O}$, respectively [32]

$$\overline{Y_S} = Y_S \frac{m}{v_F m_F} \quad (3)$$

$$\overline{Y_O} = Y_O \frac{m}{v_O m_O} \quad (4)$$

where Y_S, Y_O, m, m_F, and m_O are mass fraction of fuel, mass fraction of oxidizer, molecular weight of mixture, particle and oxidizer molecular weights, respectively.

In general, melting process of particle oxide occurs rapidly. In order to model the asymptotic melting process, Heaviside step function is used

$$\omega_{melt} = \frac{Y_s}{\tau_{melt}} H(T - T_{melt}) \tag{5}$$

where τ_{melt}, T_{melt}, T, and H represent characteristic time of melting, melting temperature of the particles, temperature, and Heaviside step function, respectively. The Heaviside step function is defined as

$$H(T - T_{melt}) = \begin{cases} 0 & T < T_{melt} \\ 1 & T \geq T_{melt} \end{cases} \tag{6}$$

Velocity field in x direction for the system is presented as [32]

$$u = -ax \tag{7}$$

where a represents the flow strain rate.

Specific heat capacity and density of the mixture are formulated as [32]

$$C = C_a + \frac{4\pi {r_p}^3 n_p \rho_p C_p}{3\rho_a} \tag{8}$$

$$\rho = \rho_a + \frac{4}{3}\pi {r_p}^3 n_p \rho_p \tag{9}$$

where C_a, ρ_a, C_p, ρ_p, r_p, and n_p represent heat capacity of oxidizing gas, gas density, heat capacity of particles, density of particles, radius of particles, and average number density of particles, respectively.

3.2. Governing equations

In order to detect distributions of temperature and mass fraction of the fuel and oxidizer in the considered zones, mass and energy conservation equations are derived. General forms of the governing equations are presented below.

Energy conservation equation is

$$-ax\left(\frac{dT}{dx}\right) = D_T\left(\frac{d^2T}{dx^2}\right) + \omega_S\frac{\mathcal{Q}}{\rho c} + \omega_{melt}\frac{\mathcal{Q}_{melt}}{c} \tag{10}$$

where D_T, ω_S, ω_{melt}, $\mathcal{Q}$, and $\mathcal{Q}_{melt}$ represent thermal diffusion coefficient, rate of reaction, melting rate of particle oxide, heat of reaction, and latent heat of melting, respectively.

Mass conservation equation for particles is

$$-ax\left(\frac{dY_S}{dx}\right) = \frac{\omega_S}{\rho} \tag{11}$$

Mass conservation equation for molten particle oxide is

$$-ax\left(\frac{dY_m}{dx}\right) = D_m\left(\frac{d^2Y_m}{dx^2}\right) + \frac{\omega_{melt}}{\rho} \tag{12}$$

where D_m represents the diffusion coefficient of molten particle oxide.

Mass conservation equation for the oxidizer is

$$ax\left(\frac{dY_O}{dx}\right) = D_O\left(\frac{d^2Y_O}{dx^2}\right) - \frac{\omega_S}{\rho} \tag{13}$$

where D_O represents the thermal diffusion coefficient of oxidizer.

In order to consider the impact of Lewis number, an effective dimensionless parameter, on the flame characteristics, the governing equations are normalized by the following dimensionless variables [32]

$$X = \frac{x}{\sqrt{\frac{\lambda}{\rho c a}}}, \theta = \frac{c(T-T_\infty)}{\mathcal{Q}Y_{S-\infty}} y_S = \frac{Y_S}{Y_{S-\infty}}, y_O = \frac{Y_O}{\vartheta Y_{S-\infty}}, y_m = \frac{Y_m}{Y_{S-\infty}}, q_{melt} \tag{14}$$

$$= \frac{\mathcal{Q}_{melt}}{\mathcal{Q}}, \tilde{\omega}_{melt} = \frac{y_S}{a\tau_{melt}} H(T-T_{melt}), \tilde{\omega}_S$$

$$= \frac{k_0 \vartheta_O Y_{S-\infty}}{\mathcal{W}_F a} y_s y_o exp\left(-\frac{T_a}{T_f}\right)$$

where θ, y_S, y_O, y_m, q_{melt}, $\widetilde{\omega}_{melt}$, and $\widetilde{\omega}_S$ are non-dimensional forms of temperature, particles mass fraction, oxidizer mass fraction, mass fraction of molten particle oxide, heat of melting, rate of melting, and rate of reaction, respectively. Also, $Y_{S-\infty}$ represents the initial mass fraction of the particles at $X = -\infty$. Following correlation is used to define the Lewis number [32]

$$Le = \frac{\alpha}{D} \tag{15}$$

where α and D represent the thermal diffusivity and mass diffusivity of fuel or oxidizer, respectively.

By applying the aforementioned dimensionless variables into the governing equations, normalized forms of the equations are rewritten as follows.

Normalized energy conservation equation is

$$\frac{d^2\theta}{dX^2} + X\frac{d\theta}{dX} + \left[\frac{\mathrm{y_S}}{a}\frac{\mathrm{H(T-T_{melt})}}{\tau_{\mathrm{melt}}}\right] = \mathcal{D}_c y_S y_O exp\left(-\frac{T_a}{T}\right) \tag{16}$$

Normalized mass conservation equation for the particles is

$$X\frac{dy_S}{dX} = \mathcal{D}_c y_S y_O exp\left(-\frac{T_a}{T}\right) \tag{17}$$

Normalized mass conservation equation for particle oxide in liquid phase is

$$\frac{1}{Le}\frac{d^2y_m}{dX^2} + X\frac{dy_m}{dX} = \frac{y_S}{a}\frac{H(T-T_{melt})}{\tau_{melt}} \tag{18}$$

Normalized mass conservation equation for the oxidizer is

$$\frac{1}{Le}\frac{d^2y_O}{dX^2} + X\frac{dy_O}{dX} = \mathcal{D}_c y_S y_O exp\left(-\frac{T_a}{T}\right) \tag{19}$$

3.3 Boundary and continuity conditions

Regarding Fig. 2, the following division is considered for the structure of the counter-flow non-premixed flame:

Preheating zone ($\mathcal{R}_1$): $-\infty < X \leq X_f^-$

Reaction zone ($\mathcal{R}_2$): $X_f^- \leq X \leq X_f^+$

Melting zone ($\mathcal{R}_3$): $X_f^+ < X \leq X_{melt}$

Oxidizer zone ($\mathcal{R}_4$): $X_{melt} < X < +\infty$

Considering the above division for the flame structure, appropriate boundary conditions are presented in Table 1.

Table 1 Boundary conditions of the combustion system.

Parameter	$\boldsymbol{X = -\infty}$	$\boldsymbol{X = X_f^-}$	$\boldsymbol{X = X_f^+}$	$\boldsymbol{X = X_{melt}}$	$\boldsymbol{X = \infty}$
θ	0	θ_p	θ_f	θ_{melt}	**0**
y_S	1	0	0	0	**0**
y_m	0	0	0	1	**0**
y_O	0	0	$y_{O.f}$	$y_{O.melt}$	$\boldsymbol{\alpha}$

where θ_p is ignition temperature of the particles. In order to enforce the continuity, calculate the locations of flame and melting fronts, and obtain the values of $y_{O.f}$ and $y_{O.melt}$, proper jump conditions at $X = X_f$ and $X = X_{melt}$ are written as

$$@\ X = X_f \implies \begin{cases} \left(\frac{1}{Le}\right)\frac{dy_O}{dX}\Big|_{X_f^-}^{X_f^+} = -\frac{d\theta}{dX}\Big|_{X_f^-}^{X_f^+} \\ \left(\frac{1}{Le}\right)\frac{dy_m}{dX}\Big|_{X_f^-}^{X_f^+} = -\frac{d\theta}{dX}\Big|_{X_f^-}^{X_f^+} \end{cases} \tag{20}$$

$$@\ X = X_{melt} \implies \begin{cases} \frac{d\theta}{dX}\Big|_{X_{melt}^-}^{X_{melt}^+} = -\frac{y_S}{a\tau_{melt}} H(T - T_{melt}) X_{melt} \\ \left(\frac{1}{Le}\right)\frac{dy_m}{dX}\Big|_{X_{melt}^-}^{X_{melt}^+} = \frac{y_S}{a\tau_{melt}} H(T - T_{melt}) X_{melt} \end{cases} \tag{21}$$

3.4. Solution of the governing equations

Using the proposed boundary conditions, normalized governing equations are solved through Matlab®. Solution of the normalized energy and mass conservation equations in each of the considered zones are presented in the following.

- Zone ($\mathcal{R}_1$): $-\infty \leq X < X_f^-$

Temperature distribution:

$$\theta = \frac{\theta_p}{[1 + erf\left(\frac{\sqrt{2}}{2} X_f^-\right)]} [1 + erf\left(\frac{\sqrt{2}}{2} X\right)] \tag{22}$$

Mass fraction of oxidizer:

$$y_O = 0 \tag{23}$$

Mass fraction of particles:

$$y_S = 1 \tag{24}$$

Mass fraction of particle oxide in liquid phase:

$$y_m = 0 \tag{25}$$

- Zone ($\mathcal{R}_3$): $X_f^+ < X \leq X_{melt}$

Temperature distribution:

$$\theta = \frac{\theta_{melt}}{[1 - erf\left(\frac{\sqrt{2}}{2}X_{melt}\right)]}[1 - erf\left(\frac{\sqrt{2}}{2}X\right)] \tag{26}$$

Mass fraction of oxidizer:

$$y_O = \frac{\left(2\left(e^{-\frac{1}{2}\frac{{X_f}^2}{1/Le}}\right)\frac{1}{Le}X + \left(-2\left(\frac{1}{Le}e^{-\frac{1}{2}\frac{X^2}{1/Le}}\right) + X\sqrt{\frac{2\pi}{Le}}\left(erf\left(\frac{X_f}{\sqrt{\frac{2}{Le}}}\right) - erf\left(\frac{X}{\sqrt{\frac{2}{Le}}}\right)\right)\right)X_f\right)y_{O,melt}}{2\left(e^{-\frac{1}{2}\frac{{X_f}^2}{1/Le}}\right)\frac{1}{Le}X_{melt} + \left(-2\left(\frac{1}{Le}e^{-\frac{1}{2}\frac{X_{melt}^2}{1/Le}}\right) + X_{melt}\sqrt{\frac{2\pi}{Le}}\left(erf\left(\frac{X_f}{\sqrt{\frac{2}{Le}}}\right) - erf\left(\frac{X_{melt}}{\sqrt{\frac{2}{Le}}}\right)\right)\right)X_f} \tag{27}$$

Mass fraction of particles:

$$y_S = 0 \tag{28}$$

Mass fraction of particle oxide in liquid phase:

$$y_m = \frac{y_{m.melt}\left(erf\left(\frac{\sqrt{2Le}}{2}X\right) - erf\left(\frac{\sqrt{2Le}}{2}X_f\right)\right)}{erf\left(\frac{\sqrt{2\,Le}}{2}X_{melt}\right) - erf\left(\frac{\sqrt{2Le}}{2}X_f\right)} \tag{29}$$

- Zone ($\mathcal{R}_4$): $X_{melt} \leq X \leq +\infty$

Temperature distribution:

$$\theta = \frac{\theta_{melt}}{[1 - erf\left(\frac{\sqrt{2}}{2}X_{melt}\right)]}[1 - erf\left(\frac{\sqrt{2}}{2}X\right)] \tag{30}$$

Mass fraction of oxidizer:

$$y_O = \frac{erf\left(\frac{X_{melt}}{\sqrt{2}}\right)\alpha + erf\left(\frac{X}{\sqrt{2}}\right)y_{O,melt} - erf\left(\frac{X}{\sqrt{2}}\right)\alpha - y_{O,melt}}{-1 + erf\left(\frac{X_{melt}}{\sqrt{2}}\right)} \quad (31)$$

Mass fraction of particles:

$$y_S = 0 \quad (32)$$

Mass fraction of particle oxide in liquid phase:

$$y_m = \frac{y_{m.melt}\left(erf\left(\frac{\sqrt{2}}{2}X\right) - 1\right)}{erf\left(\frac{\sqrt{2}}{2}X_{melt}\right) - 1} \quad (32)$$

4. Results and discussion

Chemical reaction of the considered particles with air leading to production of particle oxide is modelled as follows:

$$\varphi + (O_2 + 3.76N_2) \longrightarrow \frac{1}{2}\varphi O + 3.76N_2 \quad (32)$$

Table 2 lists the properties of particles and oxidizer used for prediction of the behavior of the counter-flow non-premixed flame.

Table 2 Input parameters considered for analysis of the system.

Parameter	Parameter defining	Value	Unit
$\boldsymbol{\rho_p}$	Density of Particle	7470	kg/m^3
$\boldsymbol{\rho_a}$	Density of gas	1.13×10^{-3}	g/cm^3
$\boldsymbol{C_p}$	Specific heat capacity of particles	654	J/kg-K
$\boldsymbol{C_a}$	Specific heat capacity of gas	1.004	kJ/kg-K

λ	Thermal conductivity	32.1	W/m.K
$\boldsymbol{Q_{melt}}$	Latent heat of melting	14.9	kJ/mol
Q	Heat of reaction	6540	kJ/kg
$\boldsymbol{T_{\infty}}$	Ambient temperature	300	K
$\boldsymbol{T_{ig}}$	Ignition temperature	900	K
$\boldsymbol{a}$	Strain rate	25	$\mathrm{cm/s}$
$\boldsymbol{\vartheta}$	Stoichiometric coefficient	2	$-$
$\boldsymbol{D_O}$	Diffusion coefficient of oxidizer	8×10^{-10}	$\mathrm{m^2/s}$
$\boldsymbol{D_F}$	Diffusion coefficient of particle	3×10^{-52}	$\mathrm{m^2/s}$
$\boldsymbol{D_m}$	Diffusion coefficient of particle oxide	4.2×10^{-7}	$\mathrm{m^2/s}$

4.1. Experimental validation

Fig. 3 shows the temperature profile of the system as a function of position (X) when radius of the particles is 3 μm. From left to right, as can be observed from Fig. 3, initial value of temperature of particles is found to be zero since their temperature is equal to the ambient temperature. As the particles move toward the flame front, their temperature increases gradually in the preheating zone. Subsequently, in the reaction zone, due to combustion of fuel and oxidizer, a dramatic increment is observed in temperature. It should be pointed out that particle oxide is the main by-product provided by the reaction of the particles and the oxidizer. Afterwards, temperature of particle oxide increases and asymptotic melting process occurs. Eventually, particle oxide in liquid phase is converted into solid phase by rejecting heat to the oxidizer stream and final temperature of the oxide will be equal to the ambient temperature. For validation purposes, simulation results of this study for temperature are compared to those obtained by Sun et al. [33]. In their experimental study, suspended particles are ignited in air in a non-premixed system. As can be observed in this

figure, temperature distributions are appropriately compatible with each other under the same condition. Based on the comparison, maximum temperature of the system obtain in the current analysis is yielded at the melting front and found to be 1420 K while maximum temperature of the system reported by Sun et al. [33] is equal to about 1400 K. The discrepancy is probably due to the structure and simplification assumptions considered for the combustion of particles in this study.

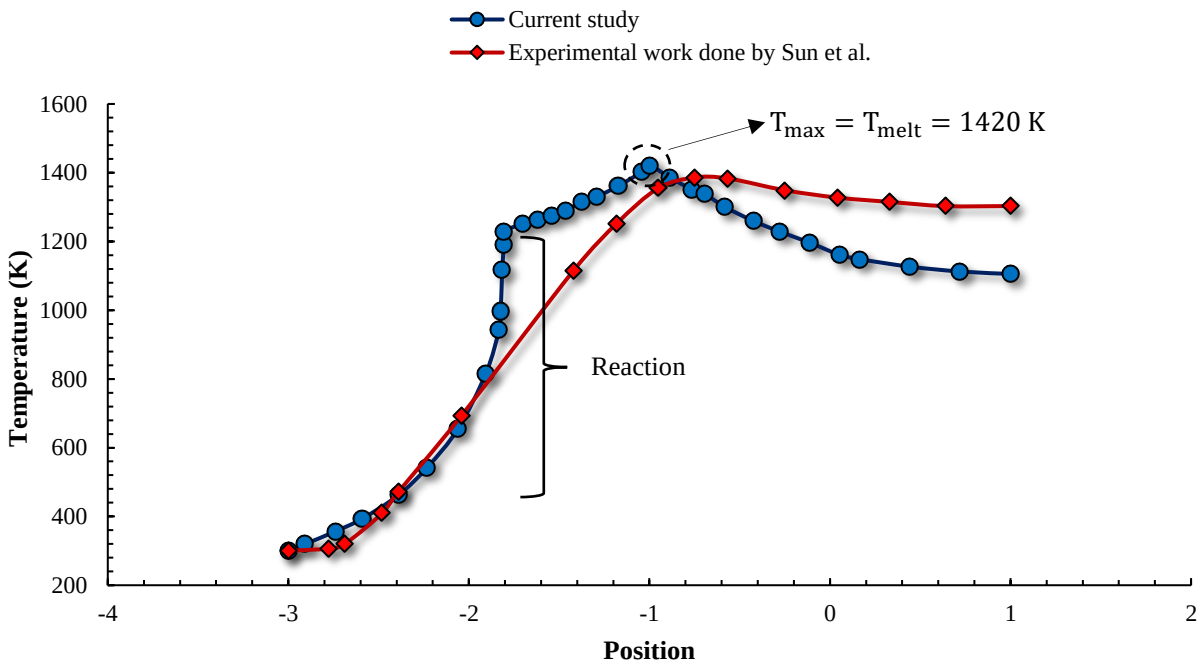

Fig. 3 Temperature distribution of the counter-flow non-premixed combustion system as a function of position.

4.2.Flame front and melting front positions

Fig. 4 delineates the flame front position as a function of Lewis number for different values of particle diameters. In order to find the locations of flame and melting fronts, a set of coupled equations are solved by Matlab® software using the jump conditions. With respect to Fig. 4, flame

front shifts toward the oxidizer nozzle with an increment in the value of Lewis number. The reason for this increase is that by increasing the value of Lewis number, mass diffusion of particles into the reaction zone reduces, as can readily be declared by the definition of Lewis number (Eq. 13). Decrement of the mass diffusion of fuel leads to a reduction in the amount of available fuel for the reaction process. Accordingly, flame temperature decreases and location of the flame front would be closer to the oxidizer nozzle. It can also be implied from Fig. 4 that an increase in diameter of the particles from 20 to 60 μm causes a shift in flame front position toward the oxidizer zone.

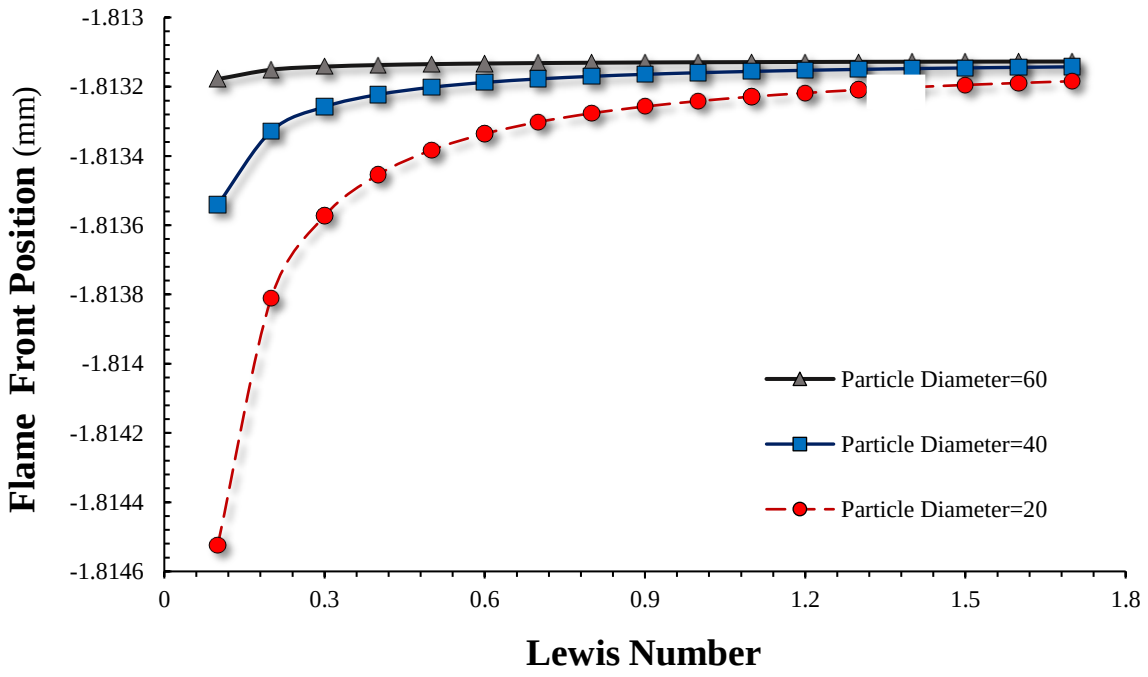

Fig. 4 Flame front position as a function of Lewis number for different diameters of the particles.

Up to now, temperature of the particles injected by the fuel nozzle has been considered to be 300 K. Figs. 5(a) and 5(b) plot the impacts of initial temperature of the particles on the positions of the flame and melting fronts for different diameters of particle, respectively. As indicated in these

figures, with an increment in the initial temperature of the particles, flame and melting fronts move toward the fuel nozzle. When the initial temperature of the particles rises, amount of heat required for reaction of the fuel and oxidizer declines. Thus, the greater the initial temperature is, the lower the values of X_f and X_{melt} are, which declares that reaction and melting processes occur more rapidly and closer to the fuel nozzle. For the investigated range of initial temperature from 275 to 315 K, the values of X_f and X_{melt} change between about -1.801 to -1.81 mm and -1.03 to -1.48 mm, respectively. According to these figures, as the size of particles increases, the amount of accessible fuel for reaction enhances resulting in decrements in values of X_f and X_{melt}.

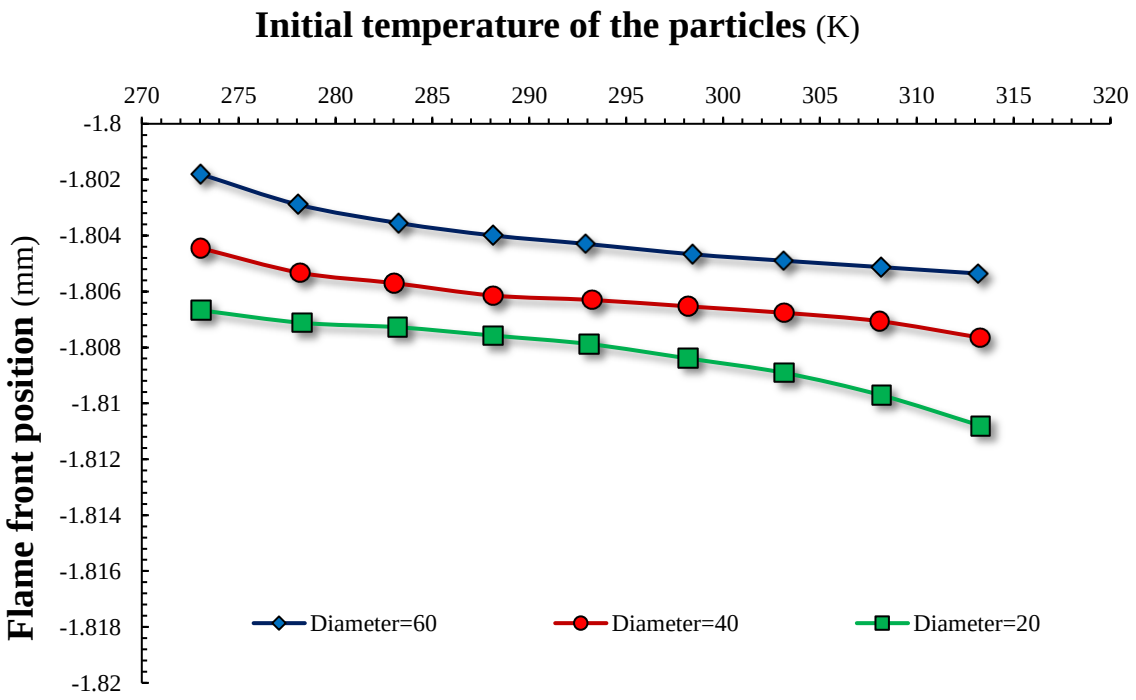

Fig. 5(a) The effect of initial temperature of the particles on the position of flame front.

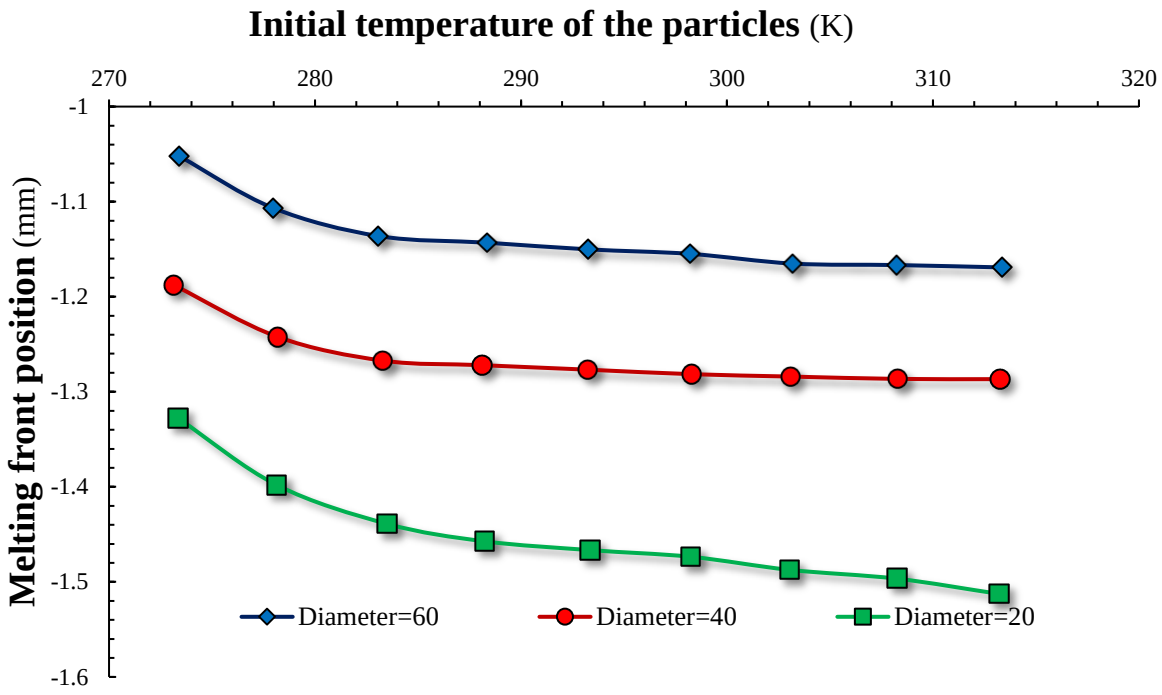

Fig. 5(b) The effect of initial temperature of the particles on position of melting front.

4.3. Mass fractions of particles, particle oxide and oxidizer

Mass fractions of the particles and molten particle oxide as a function of position are presented in Figs. 6(a) and 6(b). According to Fig. 6(a), particles are constantly heated in solid phase in the preheating zone. Then, the particles react with the oxidizer and production of particle oxide in liquid phase is started. Hence, mass fraction of the fuel particles strictly descends in the reaction zone. Figure 6(b) indicates the mass fraction of particle oxide in liquid phase at the melting front. As can be observed in Fig. 6(b), liquid particle oxide (peak of the mass fraction of molten particle oxide occurs at the melting front) is transformed into solid phase after the melting front by rejecting heat to the oxidizer flow. In this regard, mass fraction of molten particle oxide is found to be zero after the melting front.

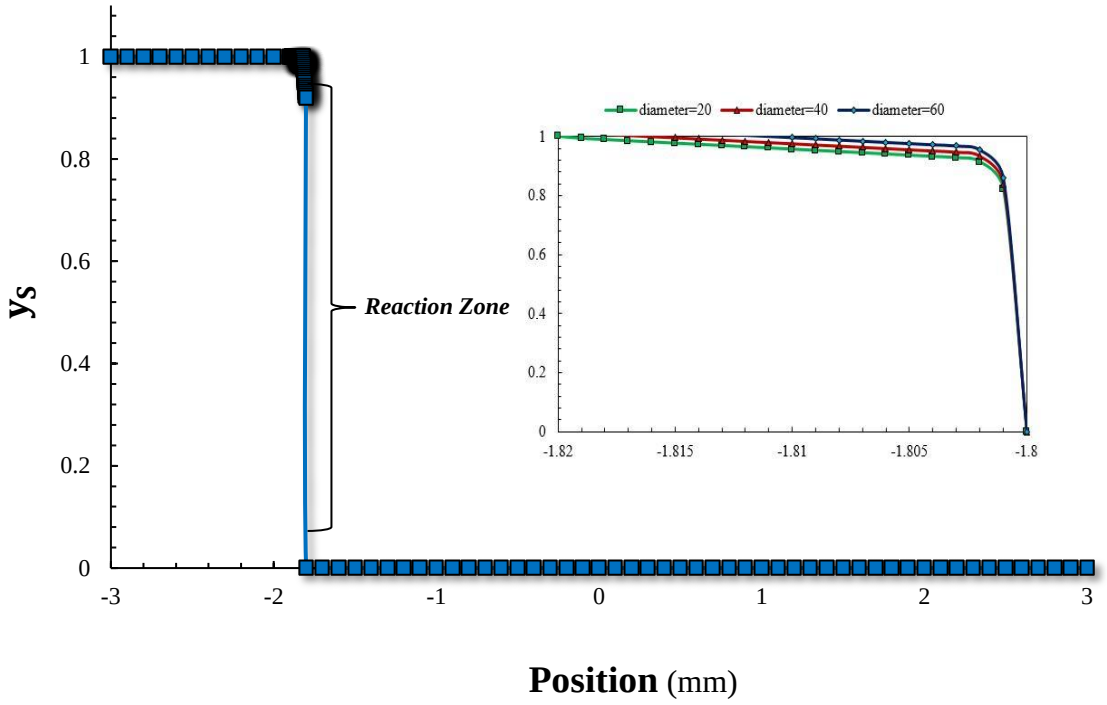

Fig. 6(a) Mass fraction of fuel in solid phase as a function of position.

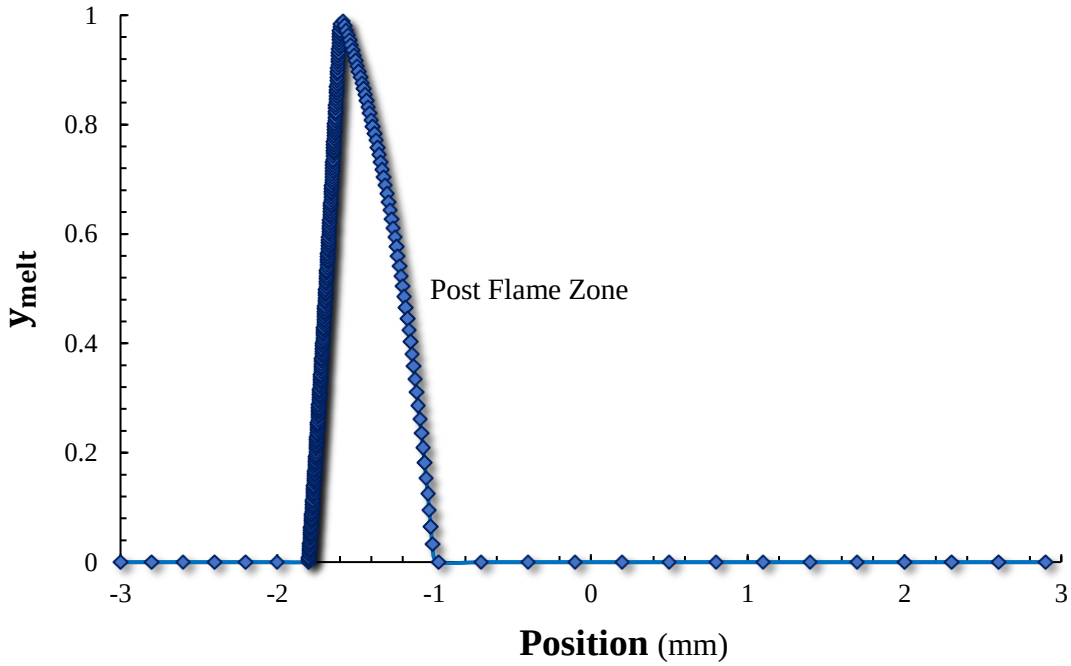

Fig. 6(b) Mass fraction of particle oxide in liquid phase as a function of position.

Figure 7(a) and 7(b) present the mass fraction of oxidizer as a function of position after the flame front for several Lewis numbers. It is notable that there is no oxidizer in the preheating zone (prior to the flame front). According to Fig. 7(a), by marching from the melting front to the flame front (oxidizer stream initially moves from left- to right-hand side through the system), mass fraction of oxidizer declines until zero. The reason for this decrement is that oxidizer is completely consumed in the reaction zone for formation of the flame. From left to right, with regard to Fig. 7(b), it can be seen that as oxidizer is consumed for production of particle oxide at the flame front, its mass fraction decreases until zero. It can also be concluded from Figs. 7(a) and 7(b) that Lewis number has insignificant effect on the mass fraction of oxidizer in the counter-flow non-premixed system.

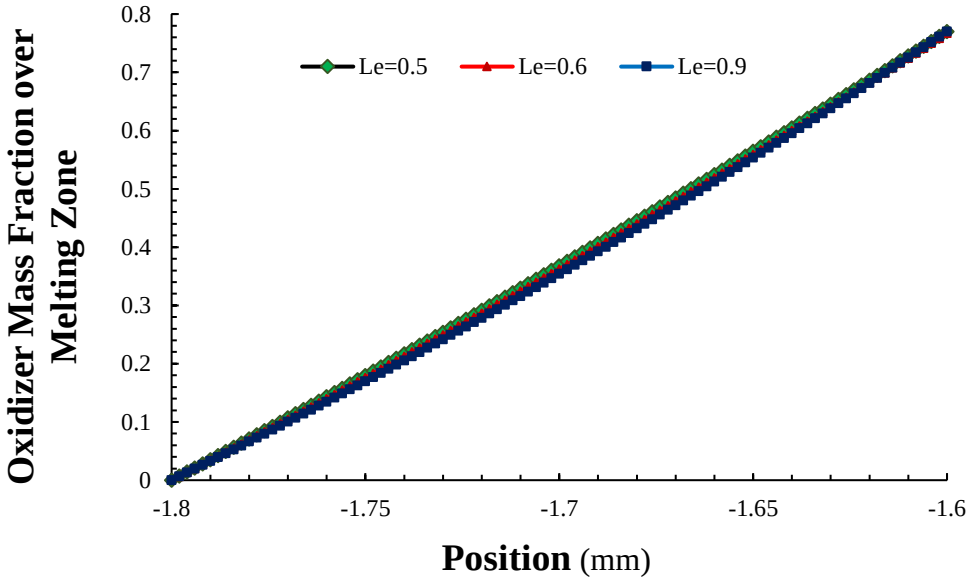

Fig. 7(a) Mass fraction of oxidizer as a function of position for the distance between flame and melting fronts.

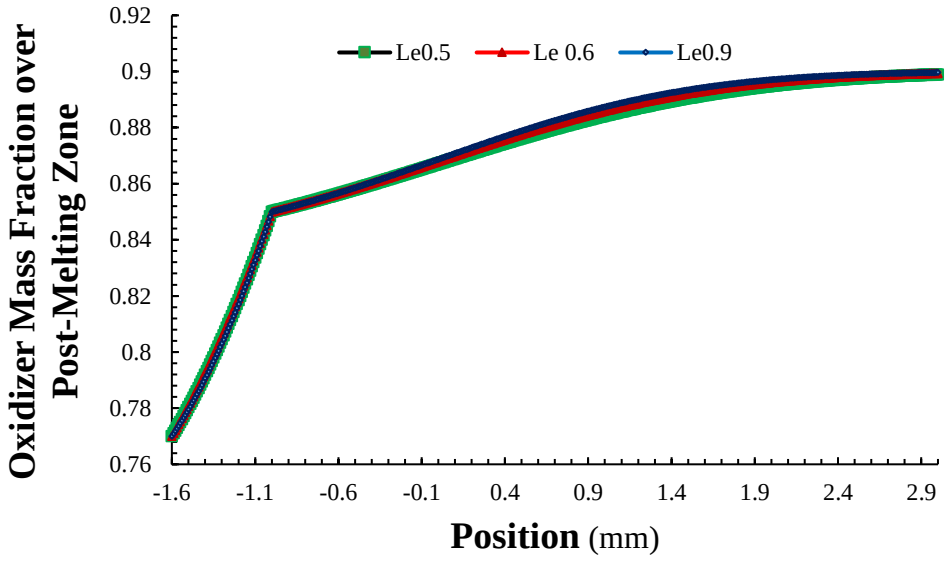

Fig. 7(b) Mass fraction of oxidizer as a function of position for the distance between melting front and oxidizer nozzle.

5. Conclusion

This study presents a counter-flow non-remixed thermo-chemical model for producing a particle oxide used in biomedical applications. Preheating, reaction, melting, and oxidation zones were analyzed using the asymptotic concept. Mass and energy conservation equations in dimensional and non-dimensional forms were derived for the system. To preserve the continuity in the system and calculate the positions of melting and flame fronts, appropriate jump conditions were proposed. According to the results, an increment in diameter of the particles would shift the flame front position toward the oxidizer nozzle. Moreover, with an enhancement in the initial temperature of the particles, flame and melting fronts moved toward the fuel nozzle. The effect of Lewis number on the mass fraction of oxidizer was insignificant in the counter-flow non-premixed system. In addition, mass fractions of the particles and molten particle oxide was slightly affected

by the size of the particles. Flame temperature and maximum temperature of the system were found to be 1310 and 1420 K, respectively. Positions of flame and melting fronts were equal to -1.8 and -1.78 mm, respectively. When the initial temperature of the particles increased from 275 to 315 K, the values of X_f and X_{melt} changed between -1.801 to -1.81 and -1.03 to -1.48 mm, respectively.

References

[1] D Shahbazi-Gahrouei, M Keshtkar; Magnetic nanoparticles and cancer treatment, *Immunopathologia Persa* 2.1 (2016).

[2] C C Berry; Progress in functionalization of magnetic nanoparticles for applications in biomedicine, *Journal of physics D: Applied physics* 42.22 (2009): 224003.

[3] S Atiq, M Z Ansar, S Riaz, S Naseem; Synthesis and characterization of magnetic nanoparticles for cancer therapy, In: *Proc. 2013 World Congress on Advances in Nano, Biomechanics, Robotics and Energy Research (ANBRE)*, 25 August, 2013.

[4] A K Gupta, R R Naregalkar, V D Vaidya, M Gupta; Recent advances on surface engineering of magnetic iron oxide nanoparticles and their biomedical applications, *Future Medicine* (2007): 23-39.

[5] W Wu, Z Wu, T Yu, C Jiang, W S Kim; Recent progress on magnetic iron oxide nanoparticles: synthesis, surface functional strategies and biomedical applications, *Science and Technology of Advanced Materials* 16.2 (2015): 023501.

[6] M Arruebo, R Fernández-Pacheco, M R Ibarra, J Santamaría; Magnetic nanoparticles for drug delivery, *Nano Today* 2.3 (2007): 22-32.

[7] E A Moacă, E D Coricovac, C M Soica, I A Pinzaru, C S Păcurariu, C A Dehelean; Preclinical Aspects on Magnetic Iron Oxide Nanoparticles and Their Interventions as Anticancer Agents: Enucleation, Apoptosis and Other Mechanism, *Iron Ores and Iron Oxide Materials* (2018): 229.

[8] S Laurent, D Forge, M Port, A Roch, C Robic, L Vander Elst, R N Muller; Magnetic iron oxide nanoparticles: synthesis, stabilization, vectorization, physicochemical characterizations, and biological applications, *Chemical Reviews* 108.6 (2008): 2064-2110.

[9] F Mata-Pérez, J R Martínez, A L Guerrero, G Ortega-Zarzosa; New Way to Produce Magnetite Nanoparticles at Low Temperature, *Advanced Chemical Engineering Research* 4.1 (2015): 48-55; DOI: 0.12783/acer.2015.0401.04.

[10] B Guo, I M Kennedy; Gas-phase flame synthesis and characterization of iron oxide nanoparticles for use in a health effects study, *Aerosol Science and Technology* 41.10 (2007): 944-951.

[11] A Ali, M Z Hira Zafar, I ul Haq, A R Phull, J S Ali, A Hussain; Synthesis, characterization, applications, and challenges of iron oxide nanoparticles, *Nanotechnology, Science and Applications* 9 (2016): 49.

[12] D Ling, T Hyeon; Chemical design of biocompatible iron oxide nanoparticles for medical applications, *Small* 9.9-10 (2013): 1450-1466.

[13] W Stumm, G F Lee; Oxygenation of ferrous iron, *Industrial & Engineering Chemistry* 53.2 (1961): 143-146.

[14] S McAllister, J Y Chen, A C Fernandez-Pello; Fundamentals of combustion processes, New York, *Springer*, 2011.

[15] M S Shadloo, Numerical simulation of compressible flows by lattice Boltzmann method, *Numerical Heat Transfer, Part A: Applications* 75.3 (2019): 167-182.

[16] M Hopp-Hirschler, M S Shadloo, U Nieken, Viscous fingering phenomena in the early stage of polymer membrane formation, *Journal of Fluid Mechanics* 864 (2019): 97-140.

[17] M S Shadloo, R Poultangari, M A Jamalabadi, M M Rashidi, A new and efficient mechanism for spark ignition engines, *Energy Conversion and Management* 96 (2015): 418-429.

[18] M Hopp-Hirschler, M S Shadloo, U Nieken, A smoothed particle hydrodynamics approach for thermo-capillary flows, *Computers & Fluids* 176 (2018): 1-19.

[19] M S Shadloo, A Hadjadj, Laminar-turbulent transition in supersonic boundary layers with surface heat transfer: a numerical study, *Numerical Heat Transfer, Part A: Applications* 72.1 (2017): 40-53.

[20] W M Daoush, Co-precipitation and magnetic properties of magnetite nanoparticles for potential biomedical applications, *Journal of Nanomedicine Research* 5.1 (2017): e6.

[21] F Mata-Pérez, J R Martínez, A L Guerrero, G Ortega-Zarzosa, New Way to Produce Magnetite Nanoparticles at Low Temperature, *Advanced Chemical Engineering Research* 4.1 (2015): 48-55.

[22] Â L Andrade, M A Valente, J M Ferreira, J D Fabris, Preparation of size-controlled nanoparticles of magnetite, *Journal of Magnetism and Magnetic Materials* 324.10 (2012): 1753-1757.

[23] H Setyawan, W Widiyastuti, Progress in the Preparation of Magnetite Nanoparticles through the Electrochemical Method, *KONA Powder and Particle Journal* (2019): 2019011.

[24] P A Dresco, V S Zaitsev, R J Gambino, B Chu, Preparation and properties of magnetite and polymer magnetite nanoparticles, *Langmuir* 15.6 (1999): 1945-1951.

[25] E M Koushika, G Shanmugavelayutham, P Saravanan, C Balasubramanian, Rapid synthesis of nano-magnetite by thermal plasma route and its magnetic properties, *Materials and Manufacturing Processes* 33.15 (2018): 1701-1707.

[26] H Rashid, M A Mansoor, B Haider, R Nasir, S B Abd Hamid, A Abdulrahman, Synthesis and characterization of magnetite nano particles with high selectivity using in-situ precipitation method, *Separation Science and Technology* (2019): 1-9.

[27] R de Almeida Silva, C D Castro, E M Vigânico, C O Petter, I A Schneider, Selective precipitation/UV production of magnetite particles obtained from the iron recovered from acid mine drainage, *Minerals Engineering* 29 (2012): 22-27.

[28] P Lei, S L Girshick, Thermal Plasma Synthesis of Superparamagnetic Iron Oxide Nanoparticles for Biomedical Applications, *Plasma Chemistry and Plasma Processing* (2012); DOI: 10.1007/s11090-012-9364-1.

[29] G I Owens, R K Singh, F Foroutan, M Alqaysi, C M Han, C Mahapatra, H W Kim, J C Knowles, Sol–gel based materials for biomedical applications, *Progress in Materials Science* 77 (2016): 1-79.

[30] M Bidabadi, P Panahifar, S Sadeghi; Analytical development of a model for counter-flow non-premixed flames with volatile biofuel particles considering drying and vaporization zones with finite thicknesses, *Fuel* 231 (2018): 172-186.

[31] M Nematollahi, H Rasam, S Sadeghi, M Bidabadi; Asymptotic prediction of multi-region planar non-premixed combustion of moisty porous coal particles in counter-flow design considering pyrolysis, homogeneous and heterogeneous reactions, *Combustion and Flame* 207 (2019): 281-294.

[32] M Bidabadi, M Ramezanpour, A K Poorfar, E Monteiro, A Rouboa; Mathematical modeling of a Non-Premixed organic Dust flame in a Counterflow configuration, *Energy & Fuels* 30.11 (2016): 9772-9782.

[33] J H Sun, R Dobashi, T Hirano; Temperature profile across the combustion zone propagating through an iron particle cloud, *Journal of Loss Prevention in the Process Industries* 14.6 (2001): 463-467.